

Chapter 9

**MASS SPECTROMETRY EVALUATION OF
THE IMPROVEMENT OF DLC FILM LIFETIME USING
SILVER NANOPARTICLES FOR APPLICATION ON
SPACE DEVICES: MATERIAL REVIEW
AND ETCHING EXPERIMENTS**

***F.R. Marciano^{1,2}, L.F. Bonetti³, R.S. Pessoa², J.S. Marcuzzo²,
M. Massi², L.V. Santos¹, E.J. Corat¹ and V.J. Trava-Airoldi¹.***

¹National Institute of Space Research (INPE), Av. dos Astronautas
1758, C.P. 515, São José dos Campos/SP, 12245-970, Brazil.

²Technological Institute of Aeronautics (ITA-CTA), São José dos
Campos/SP, 12228-900, Brazil.

³Clorovale Diamantes Indústria e Comércio Ltda, São José
dos Campos/SP, 12229-390, Brazil.

ABSTRACT

In this chapter, a review of current literature on the improvement of diamond-like carbon (DLC) films lifetime using nanoparticles, in particular, silver nanoparticles, will be presented. Studies carried out in our laboratories will also show the results of incorporating silver nanoparticles in DLC films to improve the solid lubricant's lifetime when submitted atomic oxygen bombardment. For this, etching experiments were performed in oxygen plasma operated at low pressure. The DLC films were deposited on different metallic substrates and on silicon (100) wafer with thin amorphous silicon interlayer by using a pulsed directly current plasma enhanced chemical vapor deposition discharge. During etching experiments, the films were submitted to oxygen ions with energy of ~70 eV in order to evaluate the wear process of the surface in a short period. This evaluation was conducted during and after the etching process through the quadruple mass spectrometry and profilometry techniques, respectively. With the mass spectrometry analysis was possible to monitor in real time the gas effluents during etching process as well as the main volatile compounds resultants of reactions of oxygen

with the DLC film surface like atomic carbon, carbon monoxide and carbon dioxide. The results indicate a considerably reduction of the volatile species during the etching process for samples with more concentration of silver nanoparticles. This fact is confirmed by the offline etching profile measurement which indicates a decrease in DLC etching. These results confirm that the DLC films become more wear resistant when silver nanoparticles are incorporated in the film bulk.

INTRODUCTION

Diamond-like carbon (DLC) films have a lot of technological applications due to their physic-chemical properties, such as high mechanical hardness, chemical inertness, optical transparency and wide band gap. DLC films can be produced hydrogen free named a-C, or hydrogenated named a-C:H. These films are used as protective coatings for magnetic recording media, antireflective layer for silicon solar cells and solid lubricant coating for vacuum applications. Particularly in the microelectronic industry, this material can be used as gate dielectric, inter-metal dielectric layer because of its appropriate electrical resistivity and dielectric constant. Coatings on micro machine devices are another interesting application due to low friction coefficients. As a solid lubricant coating, DLC represents an important area of investigation related to space device mechanisms, where high vacuum and atomic oxygen environments are required. The degradation of lubricants and excessive wear limit satellites and space born systems, having a number of moveable mechanical parts. Spacecraft surfaces in Low Earth Orbit (LEO), with altitudes of 200-600 km, suffer the bombardment with atomic oxygen, which is the dominant atmospheric element. Since many space systems are designed to remain active in space for 10 to 30 years, the LEO environmental presents new challenges for materials research in the development of oxidation-resistant thin-film coatings.

SOLID LUBRICANTS

Solid lubricant coatings for vacuum and space mechanisms are widely used when conventional liquid is not efficient, either when the operating conditions become too severe (aggressive etching or ultrahigh vacuum) or when a clean environment is required [1]. Liquids are used when tribo-assembly can be sealed from the outside environment. In other cases, solid lubrication is preferred [2]. Solid films may be used over a larger temperature range, but they are limited to relatively short distances of travel, less than ten million passes for rolling or sliding contacts, and relatively low speed [1].

Satellites and space-born systems have a number of moveable mechanical parts, whose reliability is severely limited by degradation of lubricants and excessive wear [2]. Satellites designed for the high vacuum of space can be exposed to moisture during assembly, ground tests, or launching, and contact atomic oxygen in LEO [2]. These extreme operating conditions are coupled with an extended service life expectancy, which could be as long as 30 years for an unattended satellite operation [2].

The mechanical, environmental, and endurance requirements of space applications exceed the available lubrication and wear reduction technologies, demanding novel materials and advanced technologies [2].

These systems are frequently tested on the ground and stored for many years under controlled environments before launching [2]. Space mechanisms are required to function in vacuum, but also during the assembly, test and storage phases which are often performed in the ambient atmosphere [1,3]. In addition, reliable data based on experimental investigations on the vibrational effects during the launching, the air-to-vacuum transition from ground to orbit, the effect of periodic temperature variations, and the action of molecular or atomic beams and particles are not completely take in account [1].

A coating can change the space-born surface (both chemistry and structure) to self-adjust to the environment and achieve long durability [2]. From the various kinds of solid lubricant coatings, it has been shown that diamond-like carbon (DLC) coatings may exhibit ultralow friction in high vacuum conditions [1,4]. DLC provide superior mechanical hardness and performance in space/terrestrial environmental cycles [2] and have been studied as potential candidate for a wear resistant material with low friction in vacuum conditions [1].

DIAMOND-LIKE CARBON

DLC is a metastable form of amorphous carbon containing a significant fraction of sp^3 bonds [5]. Carbon forms a great variety of crystalline and disordered structures because it is able to exist in three hybridizations, sp^3 , sp^2 and sp^1 [5]. According to Robertson [5], in sp^3 configuration, as in diamond, a carbon atom's four valence electrons are each assigned to a tetrahedrally directed sp^3 orbital, which makes a strong σ bond to an adjacent atom; and in the three-fold coordinated sp^2 configuration, as in graphite, three of the four valence electrons enter trigonally directed sp^2 orbitals, which form σ bonds in a plane. The fourth electron of the sp^2 atom lies in a π orbital, which lies normal to the σ bonding plane [5]. The π orbital forms a weaker π bond with a π orbital on one or more neighbouring atoms [5]. The lubricant characteristic came from the π bonds between the graphitic/diamond layer. This kind of structure (typical of graphite) confer solid lubricant characteristic to DLC.

The extreme physical properties of diamond derive from its strong, directional σ bonds [5-6]. The sp^3 bonding of DLC confers on it many of the beneficial properties of diamond itself, such as hardness, elastic modulus and chemical inertness, but these are achieved in an isotropic disordered thin film with no grain boundaries [5]. DLC consists not only of the amorphous carbons (a-C) but also of the hydrogenated alloys (a-C:H) [5].

There is a range of DLC produce methods, such as physical or chemical process. The methods can be categorized as to whether they are most suitable for laboratory studies or industrial production [5]. On a physical process, DLC film is condensed from a beam containing medium energy (~ 100 eV) carbon or hydrocarbon ions and it is the impact of these ions on the growing film that induces the sp^3 bonding [5]. This method contrasts with the chemical process in which stabilizes the sp^3 bonding [5]. On Table 1 are presenting the main features of different DLC deposition methods.

DLC films are mostly obtained by plasma decomposition of a hydrocarbon-rich atmosphere [20]. It is usually accepted that surface chemisorption of carbon carrying neutral radicals is the main channel for the film growth [20-21]. In DLC films deposited by methane decomposition, the structure is composed of sp^2 hybridized clusters interconnected by sp^3 hybridized carbon atoms. Furthermore, the mechanical properties (e.g. hardness, Young's

modulus, adhesion to the substrate, internal stresses) as well as important electronic properties (e.g. optical infrared gap, photoluminescence, conduction behavior) may be pre-determined to certain extent by varying the sp^3/sp^2 bonding ratio [5, 20].

DLC films also present low-friction coefficient, low wear rate and excellent tribological properties, as well as etching resistance [22-24]. Due to the mechanical, electrical, optical and chemical properties of these films, the use of DLC coatings in mechanical and electrical fields has increased with recent applications in food, beverage and medical application [22].

Table 1. Main features of the different DLC deposition methods.

Deposition methods	Features	Advantages	Disadvantages	References
Ion beam	Carbon ions are produced by sputtering of graphite.	Give a controllable deposition species and energy, a filtering out of non-energetic species, and the ability to dope by switching the ion species.	High cost and size of the apparatus.	[5,7-9]
Sputtering	Uses the DC or RF sputtering of a graphite electrode by na Ar plasma.	Versatility, widespread use to sputter many materials and easy of scale up.	Expensive and low growth rate.	[1,5,10-11]
Cathodic arc	An arc is initiated in a high vacuum by touching the graphite cathode with a small carbon striker electrode and withdrawing the striker.	Produce a highly ionized plasma with an energetic species, a fairly narrow ion energy distribution, and high grow rate for a low capital costs.	The filtering is not sufficient for some applications, and the cathode spot is unstable.	[5,12-14]
Pulsed laser deposition	Pulsed excimer laser such as ArF give very short, intense energy pulses, which can be used to vaporize materials as an intense plasma.	Versatile laboratory scale method, which can be used to deposit many materials, from high temperature superconductors to hard coatings.	It's not possible to scale in an industrial proportion.	[5,15-17]
Plasma enhanced chemical vapor deposition	The reactor consists of two electrodes of different area. The power supply is usually coupled on the smallest electrode on which the substrate is mounted, and the other electrode is grounded.	Versatility to use different precursor gases, facility to deposition in samples with different size and shape, low cost production.	It's not possible to have independent control of the ion current and the ion energy, as they both vary with the power supply energy.	[5,9,18-20]

In long duration, heavily loaded, and/or high sliding speed applications, the use of DLC leads to its graphitization and associated increase of friction coefficient in the high vacuum environment [2-25]. A hydrogenated DLC phase increases life through hydrogen termination of active carbon bonds, but not for long durations due to hydrogen depletion after about 10^4 cycles [2, 26-27]. An alternative approach is the incorporation of silver nanoparticles (SNP), which is also considered as a solid lubricant, into DLC films.

Diamond-Like Carbon with Silver Nanoparticles

Metal doping in DLC films prepared by chemical/physical vapor deposition techniques had been the issue of obtaining a new class of materials [28-32] but dispersing the metal particles homogeneously in the DLC matrix by the techniques used by the researches was found to be difficult [32]. The key issue was to reduce the internal stresses in DLC films via incorporation of silver nanoparticles.

In a pure carbon system, the total energy increased substantially as the bond angle deviated from the equilibrium angle of the tetrahedral sp^3 bonds, which would be the reason for the high residual compressive stress of amorphous carbon films [8]. However, the increase in the total energy was significantly reduced by the addition of noble metals as well as transition metals [8]. Choi et al suggested that both noble metals and transition metals dispersed in the amorphous carbon matrix may play the role of a pivotal site, resulting in the reduction of the residual stress in the amorphous carbon network from distortion of the bond angle [8].

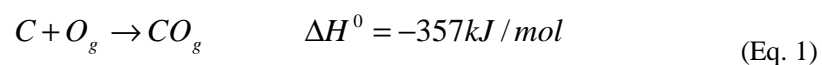
Silver is known to have low shear strength, a good transfer forming tendency, etching resistance, high electrical and thermal conductivity [7,33-34]. Furthermore, silver films produce fewer wear particles and outgas than any other material for solid lubricant while being used in a vacuum condition [7]. DLC-silver nanocomposites (Ag-DLC) have also been shown to possess antimicrobial and anticorrosion properties [8,32].

Since DLC films are large band gap material, metal inclusion in nanocrystalline form should also reveal interesting optical properties like surface plasmon resonance in this class of composite materials [32].

The Low Earth Orbit

The energetic atomic oxygen reaction with materials used in the exterior of a spacecraft operated in LEO is one of the key issues in future long-life spacecraft [18, 35]. LEO presents new challenges for materials research in the development of oxidation-resistant thin-film coatings [36]. A spacecraft in LEO environment, with altitudes of 200-600 km, suffer the bombardment by an atmosphere whose predominant species is neutral, ground-state, atomic oxygen [37-38].

The reaction of atomic oxygen with carbon,



has been described as an important process both in combustion and reentry systems [38-41]. Some researchers have been observed the removal of carbon from surfaces exposed to the atmosphere in LEO on various flights of the Space Shuttle [38, 42]. The relative kinetic energy of the atomic oxygen bombardment is approximately 5 eV which is caused by the spacecraft's orbital velocity of 400 km/h (8 km/s), and flux ranged between 10^{17} - 10^{19} atoms/m²s [43]. The high chemical reactivity of the atomic oxygen flux has been shown by the material processing experiments flown on the space shuttle [43]. Tagawa et al. reported that a pronounced glow and serious chemical etching of the surface exposed normal had been detected to the direction of flight (ram surface) [43-44]. These phenomena have been correlated with atomic oxygen density, and thickness losses over 1 μ m/day in ram surface have been observed for organic materials [43, 45-48]. These experimental data may indicate that exterior coatings used in large space structures are necessary and endurance tests against the atomic oxygen bombardments of the uncoated parts such as solid lubricants are needed [43].

Studies of the reaction of the lubricants with atomic oxygen in ground-based laboratories thus are essential to space station technologies [43]. The LEO environmental is commonly simulated in laboratory by using a standard semiconductor plasma reactor with as atmosphere of either air or pure oxygen gas [36].

The Synthesis Procedure of DLC Films with SNP

A SNP solution with about ~60 nm diameter particle was used to produce Ag-DLC films. The SNP colloidal production and nanoparticle characterization can be found in a paper previously published [49].

Silicon (100) and 316L stainless steel were the substrates. The stainless steel was polished by using up 0.25 μ m diamond powder. All the substrates cleaned ultrasonically in an acetone bath for 15 min. were mounted on a water-cooled 10 cm diameter cathode fed by a 25 KHz and 50% duty cycle pulsed directly current plasma enhanced chemical vapor deposition (DC-PECVD) power supply.

It was used two different kind of methodology to produce Ag-DLC films. On the first, SNP was interpolated into DLC in layers. On the second, SNP solution in different concentrations was pulsed during the DLC deposition process. In both cases, it was used the DC-PECVD power supply.

Ag-DLC Film Production in Layers

DLC films were deposited on silicon (100) and 316L stainless steel using a pulsed DC-PECVD methane discharge from methane (1 sccm gas flow at 85 mTorr for 10 min and -700 V). After that, the samples were divided in 5 groups. Group 1 was composed of samples with only DLC films. For the other groups, an aqueous solution with SNP was pulverized over DLC film for 2 minutes, and after this, another thin DLC layer (25 nm) was deposited to fix the nanoparticles. This procedure was carried out 4, 6, 8 and 10 times respectively for the groups 2, 3, 4 and 5.

Ag-DLC Film Production from SNP Hexane Solution

The SNP from the aqueous solution (~55 nm average size) [49] were transferred from water to hexane by centrifugation process [50]. It was obtained different concentrations of hexane SNP solutions.

The DLC films started to be deposited using methane as the feed gas to a thickness of ~150 nm (1 sccm gas flow at 85 mTorr for 10 min and -700 V). So, with the methane plasma on, hexane intermittent spray was pulsed (1 min pulse frequency and 300 μ s pulse on) inside the chamber for 25 min. The voltage (-700 V) was kept constant and the pressure inside the chamber varied from 85 to 130 mTorr during the pulse interval.

To produce Ag-DLC films, 10.0, 50.0 and 100.0 g/L hexane SNP solutions replaced the pure hexane during the deposition.

Ag-DLC Film Characterization

The morphology of SNP in DLC films was shown by scanning electron microscopy (SEM) in Figures 1-2 and by atomic force microscopy (AFM), Figure 3-4. SEM images were acquired by using JEOL LEO-440, with 20.0 kV; and field emission gun scanning electron microscopy (FEG-SEM), JEOL JSM-6330F, with 30.0 kV, respectively. The AFM images were acquired by using the dynamic tip mode of a Shimadzu SPM9500J3 and VEECO 920006101 AFM, respectively.

The nanoparticle size is in good agreement with the SNP size in solution. Different sizes and shapes of SNP are also shown. As illustrated in Figure 1-2, it was possible to reach a satisfactory density of nanoparticles with the adopted methodology. The images reveal that SNP are not dispersed absolutely homogeneously. One may observe that two or more nanoparticles may be representing a large particle.

AFM images (Figures 3-4) confirmed SNP were really incorporated in DLC films. The nanoparticles had a tendency to form aggregates on the surface during the deposition process [51] (as shown on top right side of Figure 3a). Secondly, Figure 3b shows some nanoparticle completely immersed in DLC films and others partially immersed in DLC surface. SEM and AFM images shows the tendency of the inter-particle distances became smaller with the increase in number density of particles culminating in some clusters coming closer to one another.

On Ag-DLC films produced from SNP hexane solution (Figure 4), the agglomerate problem becomes more evident. This can be seen in Figure 4b (DLC from 50.0 g/L SNP hexane solution) which has not only more SNP, but also more agglomerates than on Figure 4a (DLC from 10.0 g/L SNP hexane solution). In the case of Figure 4, the SNP are bigger and form more aggregates on DLC surface, which can mislead the SNP real sizes. However, DLC films growth from hexane have higher growth rates, it means this methodology is more applicable when industrial scaling up is taking in account.

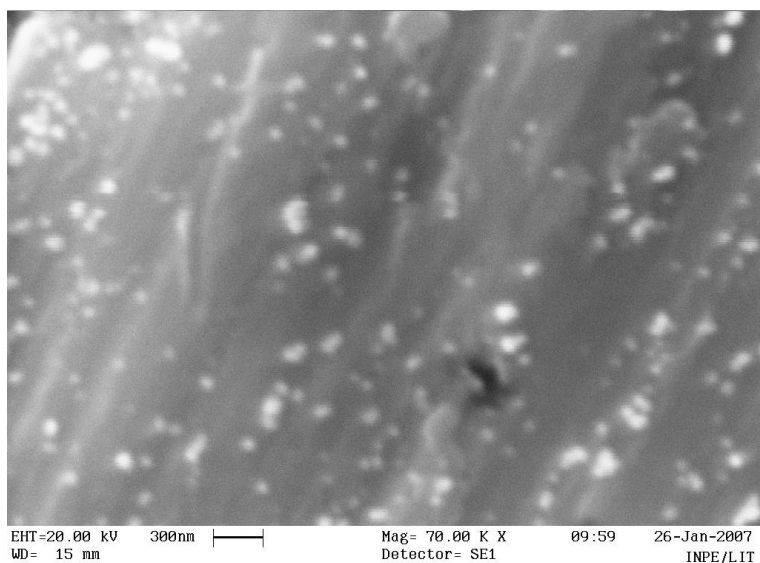


Figure 1. SEM image of a 10-layer-Ag-DLC film.

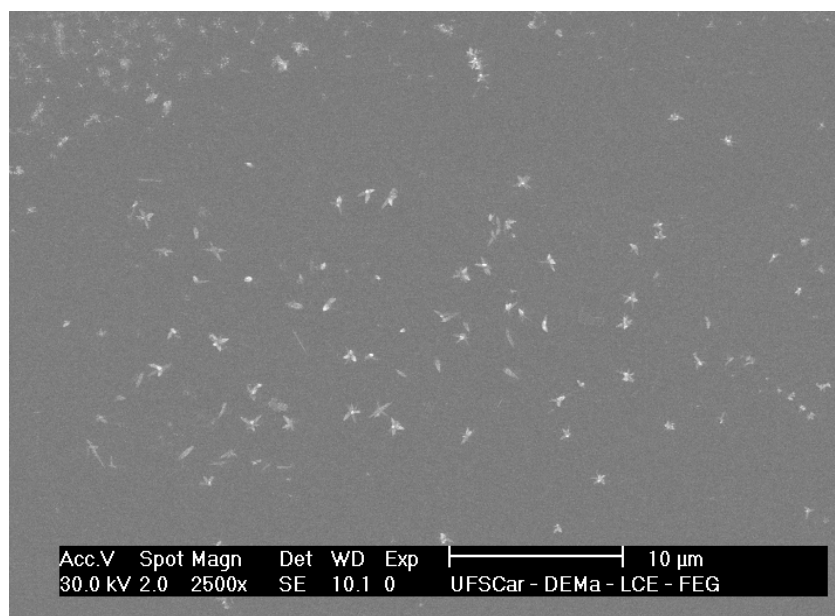


Figure 2. SEM image of Ag-DLC film produced from a 10.0 g/L SNP hexane solution.

The atomic arrangement of the Ag-DLC films was analyzed by Raman scattering spectroscopy in order to verify if the incorporation of SNP in DLC changed its arrangement using a Renishaw 2000 system with an Ar⁺-ion laser ($\lambda = 514$ nm) in backscattering geometry. The laser power on the sample was ~ 0.6 mW and the laser spot had 2.5 μm diameter. The Raman shift was calibrated in relation to the diamond peak at 1332 cm^{-1} . All measurements were carried out in air at room temperature.

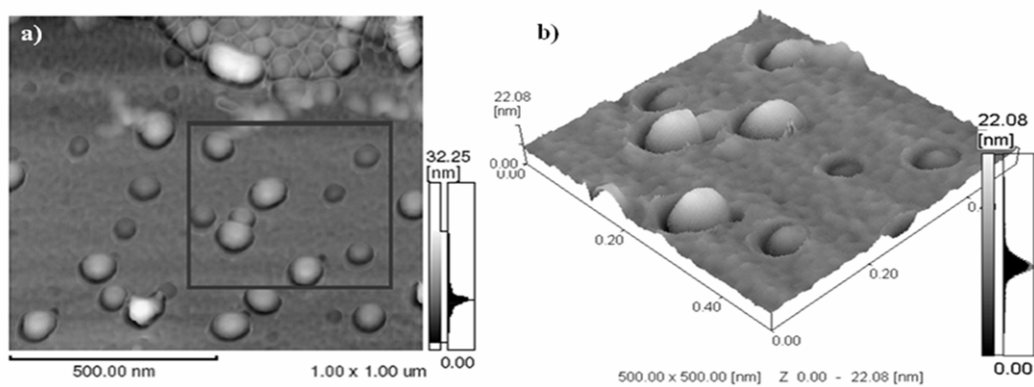


Figure 3. 10-layer-Ag-DLC film AFM image: a) 2D AFM using the dynamic tip mode in 500×500 nm² area and 22.08 nm depth. b) 3D enlargement of the squared region delineated in (a).

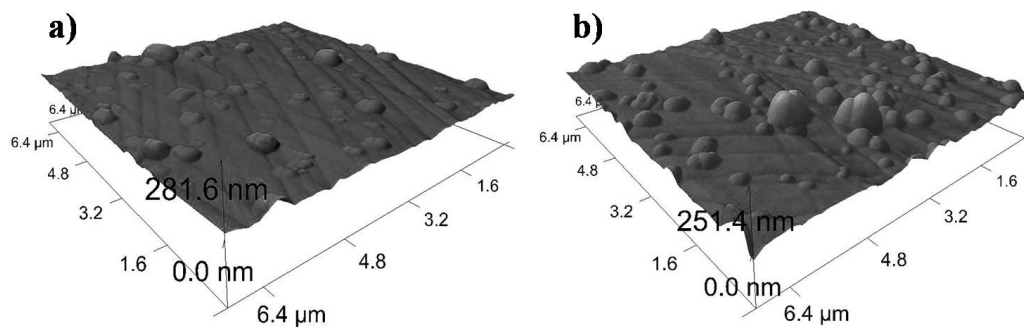


Figure 4. AFM image of Ag-DLC film produced from (a) 10.0 g/L and (b) 50.0 g/L SNP hexane solution.

Figure 5 shows Raman spectra of a pure DLC film and a 10-layer-Ag-DLC film. The two spectra are very similar. Presenting two overlapping bands known as the *D* and *G* bands [52], these spectra were fitted using two Gaussian lines. The integrated intensity ratio of the *D* and *G* peaks (I_D/I_G) has been correlated with the sp^3/sp^2 bonding ratio [53-54]. $I(D)/I(G)$ falls as the number of rings per cluster and the fraction of chain groups rise [55]. The measured I_D/I_G ratios for these quality DLC films ranged between 1.0 and 1.2 and these values do not change according with the Ag quantity tested. They are common values for DLC films [55] and these parameters are empirically correlated to quantities directly related to structural disorder, such as the Young's modulus, the hardness, hydrogen content, and atomic density [56]. Choi et al (2008) show I_D/I_G ratio increases as the Ag contents in the DLC film increases. In that case, Ag-DLC films were produced from a hybrid deposition system composed of an end-Hall-type hydrocarbon ion gun and a silver DC magnetron sputter source [57]. From these results, it is noticeable the quality of DLC films do not suffer any variation with the incorporation of SNP, independent of both used methodology.

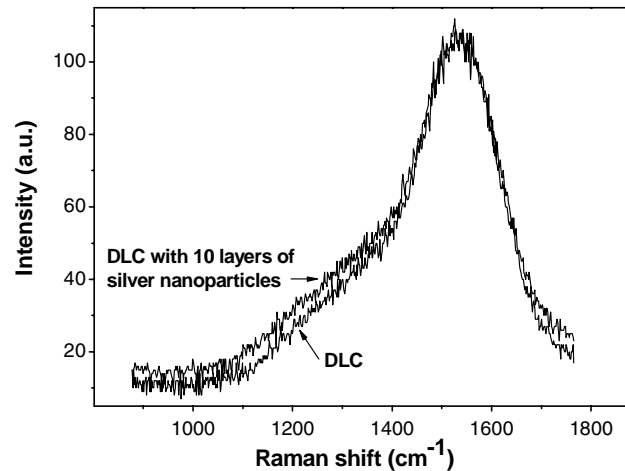


Figure 5. A comparison between Raman spectra from DLC without and with 10 layers of SNP.

Some authors [8,32] reported the stress reduction via nanoparticle incorporation in DLC bulk. Total stress was determined by measuring the substrate curvature before and after the DLC film deposition with a stylus profilometer and by analyzing the results with the well-known Stoney's equation [58-59].

Figure 6 shows the total compressive stress of the DLC films measured according to the layers. The zero point corresponds to the pure DLC film without any layer. The stresses of the films with SNP were decreasing with the number of silver layers whilst in the films with no silver, the stresses remain constant independently of the number of layers. SNP in DLC bulk also relieve the stresses between the substrate and DLC films. Lower total stress observed when nanoparticles are present in the DLC films are related to the defects in the films structure and multi-layer of the DLC films.

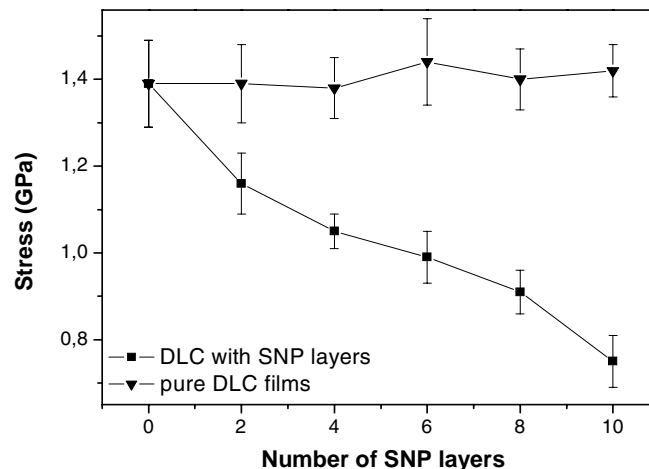


Figure 6. Total compressive stress as a function of the number of SNP layers. The zero point corresponds to the pure DLC film without any layer.

Table 2. DLC and Ag-DLC hardness values (in GPa).

Production method	DLC	Ag-DLC
In layers	18-22	11-16
From hexane solution	18-20	11-14

Oxygen Plasma Etching of DLC and Ag-DLC Samples: Plasma Reactor and Discharge Parameters

Nanohardness was measured by the instrumented hardness test which was carried out using Fischerscope HV100 equipment with a Vickers indenter. The maximum load applied was 45 mN and at least 10 valid measurements were made for each sample. The hardness mean value was considered as the resultant hardness. The depth achieved was less than 20% of total film thickness in order to avoid substrate influence during the measurements. The load-unload cycles and hardness values were performed according to ISO 14577 [60] and the Oliver-Pharr method [61].

The DLC and Ag-DLC hardness values are presented on Table 2, according to the deposition method (in layers or from the hexane solution). When SNP are incorporated, DLC hardness also present a slightly decrease, because it was added a lot of defects in DLC structure. This decrease in hardness is counterbalanced with the increase of other properties of these films such as lower stress [49]. The difference in hardness among the films with SNP was not significantly different.

The etching of carbon based materials, like DLC films, can be done with discharges operating at two regions of pressure: atmospheric and low pressure oxygen plasmas. The atmospheric plasma generator proposed by Marcuzzo et al [62] consists in the use of dielectric barrier discharge (BDB) in oxygen gas at high pressure (600 Torr) and high gas flux (3 L/min). Despite this method can produce reactive oxygen, it was not used because the high gas flux and pressure not represent the LEO conditions.

Under low pressure (< 1 Torr) of reactive gases such as oxygen is common the use of techniques that use 13.56 MHz radio-frequency (RF) power sources to excite the plasma generation such as reactive ion etching (RIE), inductively coupled plasma (ICP) and electron cyclotron reactor (ECR) [63]. In this work we used the RIE system due to simplicity of construction and ability to generate oxygen plasma at pressures that simulate the LEO conditions. A schematic diagram of the experimental apparatus is shown in Figure 7. This apparatus consists of a capacitively coupled parallel plate reactor operating in RIE mode with 2 L volume and 50 mm electrode gap. The lower RF powered electrode has 150 mm in diameter while the upper electrode is connected with the reactor walls and grounded. Prior to gas feed the vacuum chamber is pumped down to pressure below 0.1 mTorr using a combination of a roots and a mechanical pump, providing both an effective pumping speed of approximately 110 L/s. Subsequently, the O₂ was inserted into the chamber.

For the etching experiments the DLC or Ag-DLC films were placed on the lower electrode since this enables the control of the flow and energy of species such as ions and charged electron on the sample through the modulation of process parameters such as

pressure and RF power. All data were taken at an optimized condition of 20 mTorr total pressure (12 sccm gas flow) and 10 W of RF power. Under these conditions the established cathode fall potential (V_{dc}) is of the order of 70 V, which is equivalent to an energy gained by oxygen ions of 70 eV. In LEO simulator studies, the particle energies involved are about 5 eV, which promotes a slow etching process [38]. In our experiments, the high energy was chosen purposely in order to maximize the etching process quickly. Etching experiments were carried out through on masked DLC samples for 4 min, and part of them was covered with a mechanical mask to produce a step between the etched and non-etched regions. This step was measured by a profilometer (Alpha-Step 500), and the etching rates were determined.

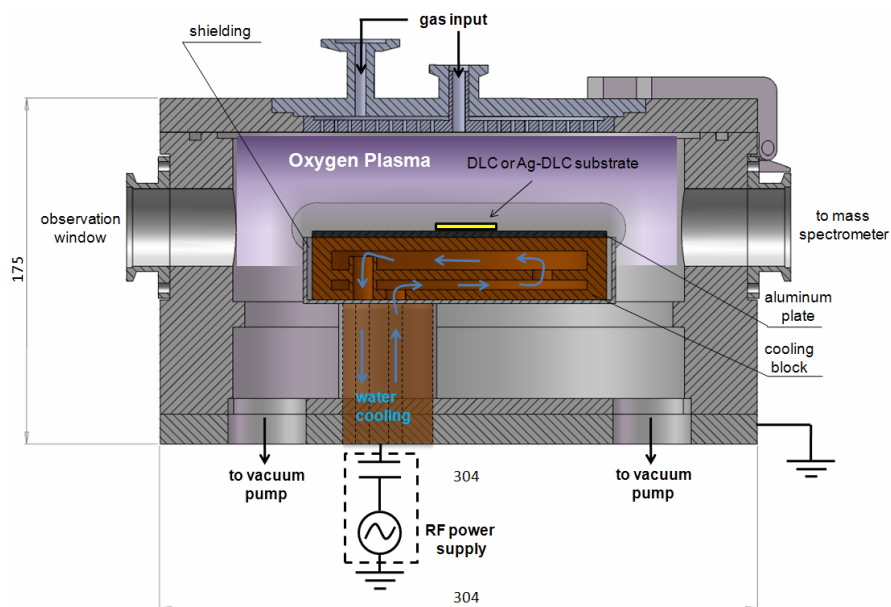


Figure 7. Schematic illustration of the reactive ion etching reactor. The reactor dimensions are in mm.

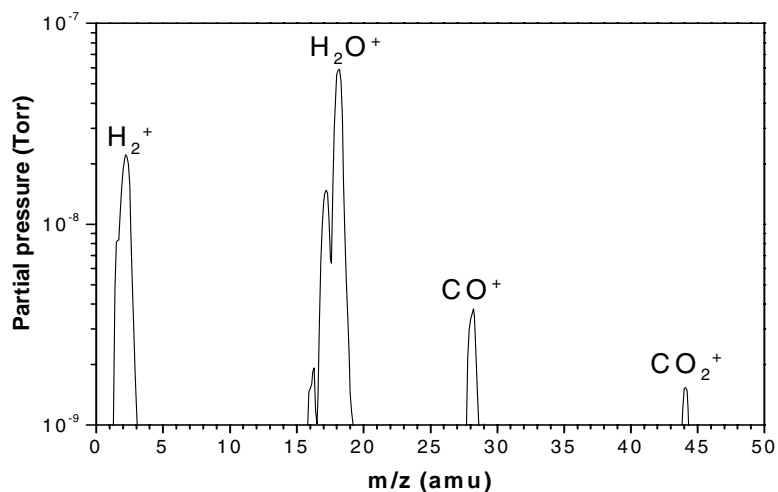


Figure 8. Mass spectrum of the RIE chamber obtained on background condition.

In Situ Plasma Etching Analysis: The Mass Spectrometry Technique

The mass spectrometry is a powerful analytical technique that is used to identify unknown compounds, to quantify known materials, and to elucidate the structural and chemical properties of molecules. The detection of compounds can be achieved, even in very small quantities (partial pressures of up to 10^{-10} Torr). Because of this, the mass spectrometry provides valuable information for a wide range of professionals: physicians, engineers, chemists, biologists and astronomers, to name a few.

One method that uses frequently the mass spectrometry to perform their diagnosis is the processing of materials by cold plasma. However, determining the chemical composition of plasma is a very difficult task, due to the large amount of components and radicals present. In reactive plasmas such as O_2 , SF_6 or CF_4 , for example, the knowledge of the absolute concentrations of chemical species involved is extremely complicated, why, in many cases, only magnitudes are measures relating experimentally. In a reactive discharge, the energy is distributed among the various constituents, namely: stable neutral, electrons, molecular fragments (radicals), negative and positive ions and neutral excited. These, in turn, are in a chemical "soup" of large applications in various branches of technology. Of these components, it should be emphasized that the role of electrons, because of its greater mobility, are responsible for the electrical conductivity of plasma and the processes of formation of radicals, neutral and excited ions, important for the reactivity of the plasma.

In this scope, in the field of plasma etching of materials, particularly, etching of carbon-based materials, the use of mass spectrometry allows the monitoring of neutral effluents like atomic carbon, carbon monoxide and carbon dioxide that are generated during the reaction of oxygen plasma species with the substrate. The knowledge of these species allowed us to this work not only investigates the process kinetics but also evaluate the wear resistance of each material.

Quadrupole Mass Spectrometer System

The analysis of the relative concentration of species extracted from the plasma was performed by using a quadrupole mass spectrometer AccuQuad 200D – Kurt J. Lesker Company, which allows to analyze mass up to 200 atomic mass unit (amu) with a resolution 1 amu, adapted to the vacuum chamber through a drifting tube. The plasma species were sampled through a micro orifice located at the mass spectrometer's entrance, undergoing subsequent electron impact ionization at constant electron energy of 70 eV. This energy is sufficient to ionize the neutral gas species that enter through the quadrupole RF mass filter that thus, is detected and classified as a function of their mass-to-charge ratio. The typical operation pressure within the mass spectrometer was 0.1 mTorr.

Mass Spectra Analysis Procedure

The first instance of a mass spectrometry analysis in cold plasma reactors is an inspection of the residual species inside the reactor in order to avoid these from the species of gas to be inserted. These species are illustrated in the spectrum shown in Figure 8. In this spectrum we

can see that the reactor was clean, i.e., without the presence of etching gas at a background pressure of approximately 0.1 mTorr. The species that can be observed in spectrum probably are contaminants that may be associated with small leaks in the reactor and because polypropylene pipelines that are used as drivers of gas, and yet there is the presence of water (mass 18) that probably should be constituent of the ambient air. This procedure has been taken aimed at determining the background conditions for subsequent analysis.

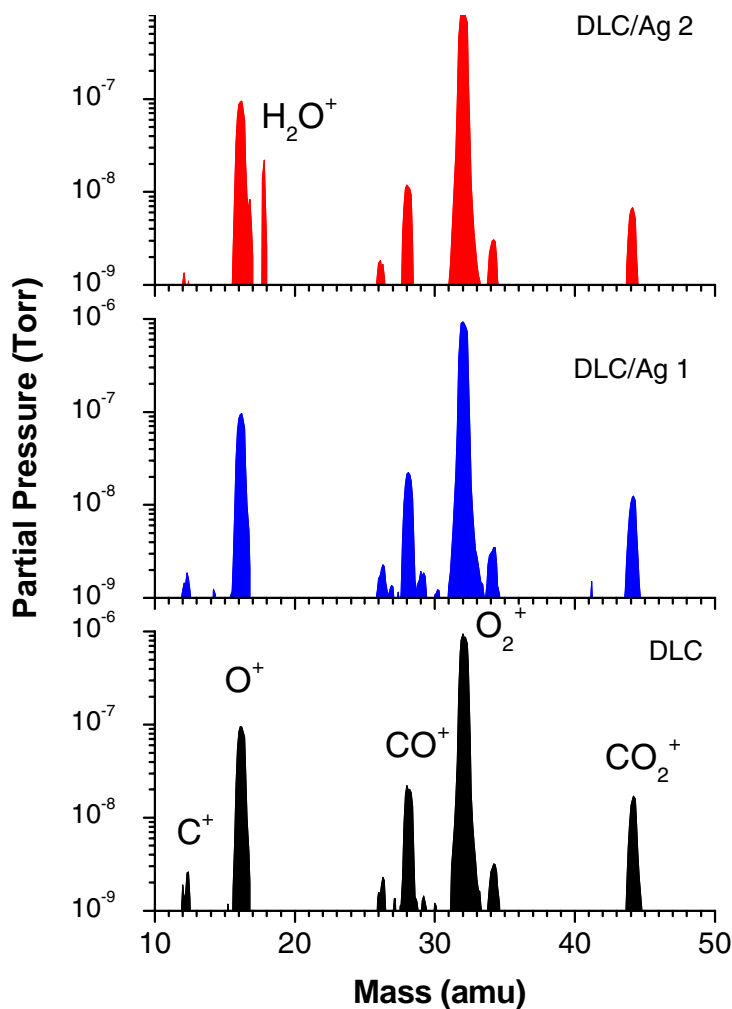


Figure 9. Mass spectra of the effluent from the reactor during etching of DLC and Ag-DLC films.

Once the subtraction of the background spectrum was made, we conducted the online monitoring of the etching process of DLC and Ag-DLC materials. Figure 9 illustrates an example of the spectra obtained for 3 different samples: DLC, Ag-DLC with 1 layer and Ag-DLC with 2 layers. We observed the following main species in these spectra: O^+ (mass 16) and O_2^+ (mass 32), from the oxygen gas and C^+ (mass 12), H_2O^+ (mass 18) and CO^+ (mass 28), from the reaction of oxygen species with the surface of the DLC substrate. The atomic carbon observed in gas phase derives from the reactive sputtering effect in the material

surface due to bombardment by oxygen ions with energies of up to 84 eV. This effect decreases when the silver layers in the film bulk increases. Also, it was observed from these spectra a decrease in the partial pressure of CO^+ and CO_2^+ species which allows us to conclude that the reaction rates to formation of these species in gas phase are diminishing because the capture of oxygen by silver nanoparticles.

Etching Results for Ag-DLC Film in Layers

In order to verify the effect of the number of SNP layers on the generation of C^+ , CO^+ and CO_2^+ species, experiments were done varying the number of layers from 0 to 10. Figure 10 shows the normalized partial pressure of C^+ , CO^+ and CO_2^+ species as a function of the number of SNP layers. It noted a signal value strong decrease for the films with more than 4 SNP layers, where the signals decrease to 2 times up for the case of 10 SNP layers.

The mass spectrometry results observed during the etching process were corroborated by measuring of the etching step formed by a mask placed over a small area of the substrate. The height of these steps were measured after the process by a profilometer and so were determined the etching rates for each condition. The results are shown in Figure 11, the obtained etching rates are presented as function of the number of SNP in DLC film. In Figures 10-11, the zero point corresponds to the DLC film without any layer of SNP. As can be observed from Figure 11, a decrease in the etching rate up to 2 times occurs for value of 10 SNP layers. This fact shows the effectiveness of the mass spectrometry technique to evaluate the wear resistance of Ag-DLC material to the oxygen etching process.

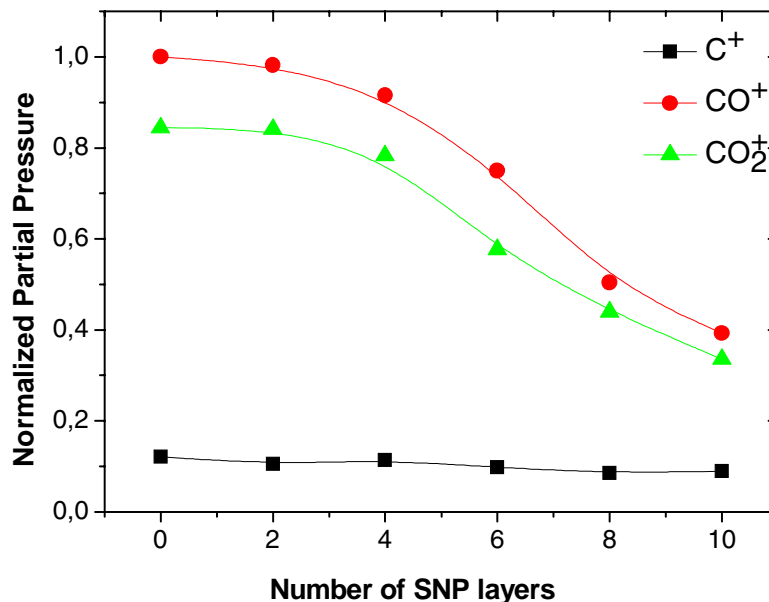


Figure 10. Normalized partial pressure of C^+ , CO^+ and CO_2^+ species as a function of the number of SNP in DLC film. Partial pressures are normalized to 1 at the maximum value.

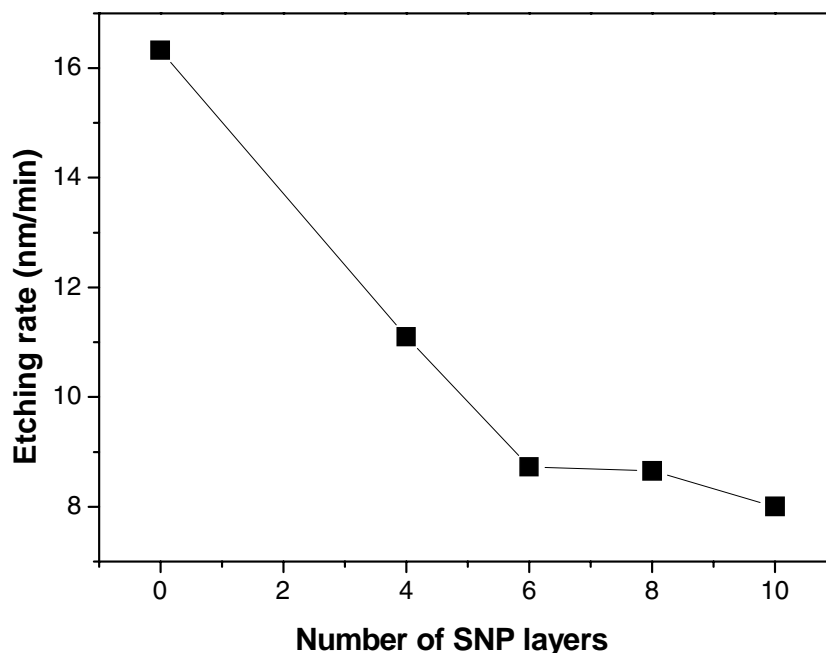


Figure 11. Etching rate as function the number of SNP layers in DLC films.

Etching Results for Ag-DLC Film from SNP Hexane Solution

Figure 12 shows the obtained etching rates as function of SNP concentration in hexane solution. The etching shows that with an addition of 10.0 g/L of SNP in hexane, the etching rate suffers a decrease of more than 2 times of initial value, reaching a decrease of up to 3.5 times to a maximum hexane solution concentration of 100 g/L.

Also for this case, we have made the process monitoring by mass spectrometry, but with one difference, the main etching species CO^+ and CO_2^+ are monitored in real time at an interval range of 1 second between each detection. This permitted us to see how the signals of the species varies during all etching process, allowing a better evaluation of the effect of the silver concentration on the wear of the film. In Figure 13, the time evolution of CO^+ and CO_2^+ species is presented during the oxygen plasma degradation for DLC samples produced for (a) pure hexane, (b) 10.0 g/L SNP hexane solution, (c) 50.0 g/L SNP hexane solution and (b) 100.0 g/L SNP hexane solution. In this figure, on point 1, oxygen gas had started to be inserting in the chamber, point 2, plasma (10 W) had been on, and, point 3, plasma and oxygen had been off. We can see that when the discharge is on, a significant increase in the partial pressure of CO^+ and CO_2^+ species can be observed, indicating the reaction of oxygen species with the substrate material. After the discharge ignition the signals tends to decrease rapidly with time indicating a constant decrease in etching rate. This fact shows to be more prominent for higher silver concentrations.

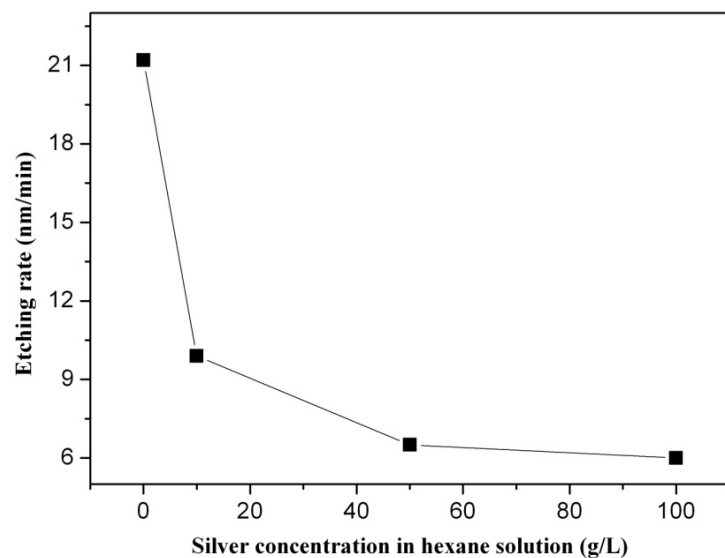


Figure 12. Etching rate as function of SNP concentration in hexane solution.

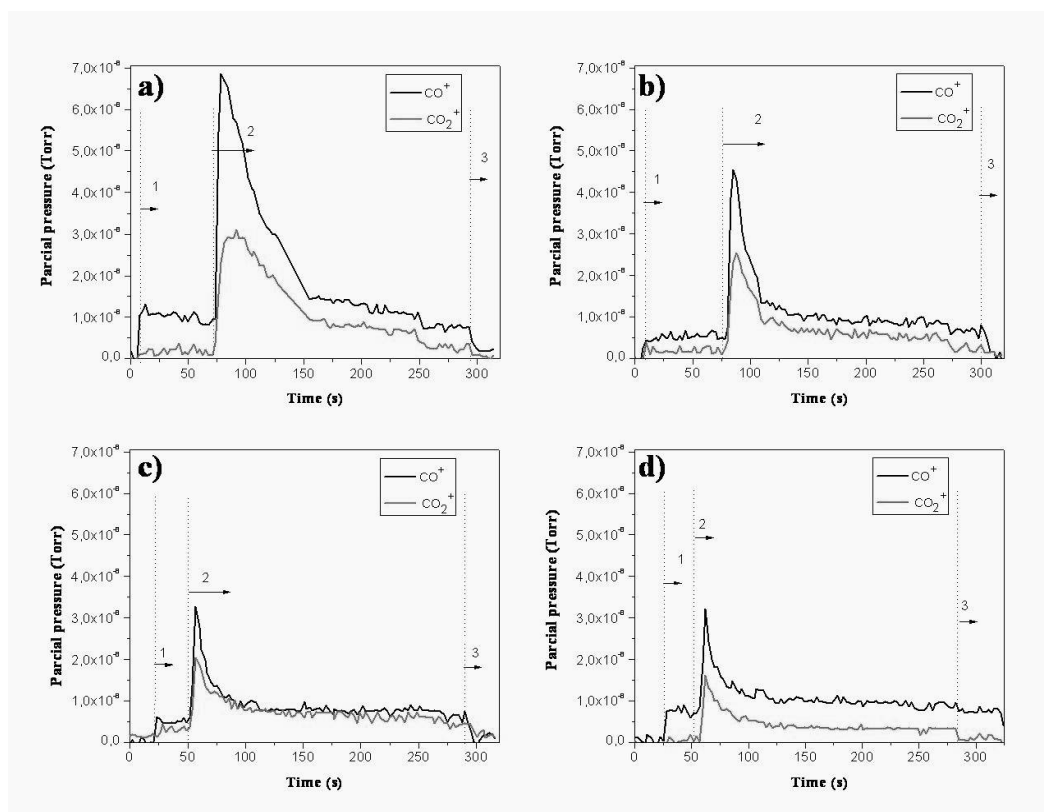


Figure 13. Temporal evolution of CO^+ e CO_2^+ species during the etching process of the DLC films produced from (a) pure hexane, (b) 10.0 g/L SNP hexane solution, (c) 50.0 g/L SNP hexane solution, and (d) 100.0 g/L SNP hexane solution. On point 1, oxygen gas had started to be inserting in the chamber, point 2, plasma (10 W) had been on, and, point 3, plasma and oxygen had been off.

It is known from the literature, that the etching process of the DLC material by cold plasmas is performed with the use of oxygen gas [64]. This, due to reaction with carbon, promotes the generation of volatile products CO and CO₂ that are pumped out by the vacuum system. With the insertion of SNP in the film volume, independent of the used method, the etching process of the film becomes slower, since silver has a higher reaction affinity with oxygen atoms forming a silver oxide layer on DLC surface owing to the irradiation of oxygen plasma. Oxygen atoms react preferentially with silver preventing the reaction of oxygen with carbon from the DLC films. The result of this experiment can be seen in Figures 11 and 12. Here, the obtained etching rate decreases with the increase of SNP in DLC bulk. The increase of SNP in the film proved to be very efficient in reducing the reaction of oxygen with carbon. This result was also verified by the analysis of etching environment with mass spectrometer (see Figures 10 and 13). The partial pressure of CO⁺ and CO₂⁺ showed a decreased with the increase of SNP, indicating that the film etching decreases with the increase of SNP. This decrease in the etching rate is due to the fact of rising silver agglomerates on the film surface as we can see in images of optical microscopy of Figure 14. One can note on the etched samples, that the silver nanoparticles become more evident, having resisted the etching process. In such case, the DLC films with silver nanoparticles become more resistant to the etching process allowing an increase of DLC permanency at the space atmosphere.

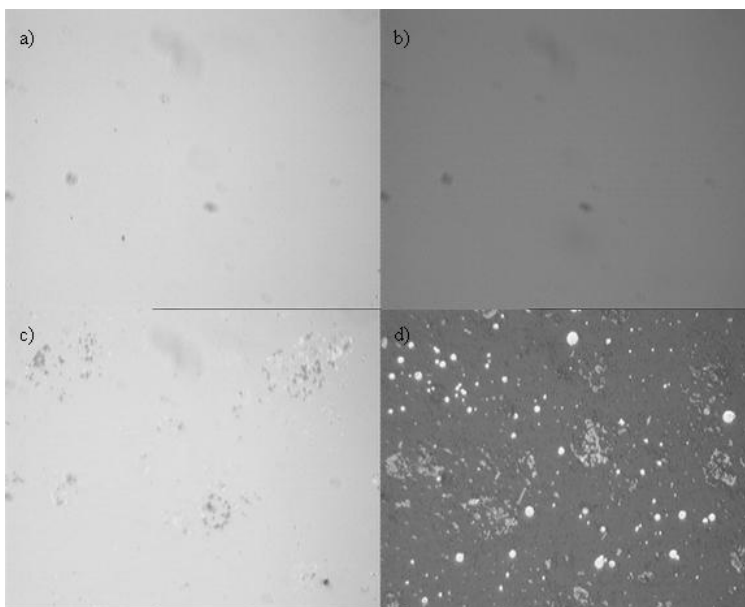


Figure 14. Optical microscopy of some samples before and after the etching process: a) DLC film before the etching, b) DLC film after the etching, c) 8-layer-Ag-DLC film before the etching, d) 8-layer-Ag-DLC film after the etching. All the figures are in the amplification of 1000x.

CONCLUSION

The SNP incorporation technique in DLC bulk presented in this chapter shows high quality Ag-DLC films produced. Raman scattering spectra shows DLC quality does not suffer

any significant variation with the SNP incorporation. Also demonstrated that DLC films are more wear resistant against etching when the films have more SNP. It is clear the amount of CO₂ and CO produced by oxygen ion attack decreases with the increase of SNP in DLC bulk. We are convinced SNP react with oxygen, absorbing the oxygen atoms close to the DLC films surface. The mass spectrometry analysis was an indispensable technique to identify and to quantify the compounds etched by the oxygen plasma.

This chapter is part of initial studies to understanding this kind of etching process. Therefore, more experiments are need in order to further investigation the SNP behavior in DLC films and its effect on the etching process, as a function of SNP size and density.

REFERENCES

- [1] Donnet, C; Fontaine, J; Le Mogne, T; Belin, M; Héau, C; Terrat, JP; Vaux, F; Pont, G. *Surf. Coat. Technol.*, 1999, 120-121, 548-554.
- [2] Voevodin, AA; Zabinski, JS. *Compos. Sci. Technol.*, 2005, 65, 741-748.
- [3] Rountree, RA. *J. Mech. Eng.*, 1988, 35, 28-32.
- [4] Donnet, C; Grill, A. *Surf. Coat. Technol.* 1997, 94-95, 456-462.
- [5] Robertson, J. *Mater. Sci. Eng. R* 2002, 37, 129-281.
- [6] Angus, JC; Hayman, CC. *Science* 1988, 241, 913-921.
- [7] Lee, KH; Takai, O; Lee, MH. *Surf. Coat. Technol.* 2003, 169-170, 695-698.
- [8] Leger, LJ. et al. AIAA paper no. 83-2631 (1983).
- [9] Choi, HW; Choi, JH; Lee, KR; Ahn, JP; Oh, KH. *Thin Solid Films*, 2007, 516, 248-251.
- [10] Trava-Airoldi, VJ; Bonetti, LF; Capote, G; Santos, LV; Corat, E. *J. Surf. Coat. Technol.* 2007, 202, 549-554.
- [11] Lu, ZG; Chung, CY. *Diamond Relat. Mater.*, 2008, 17, 1871-1876.
- [12] Ji, L; Li, H; Zhao, F; Chen, J; Zhou, H. *Diamond Relat. Mater.*, 2008, 17, 1949-1954.
- [13] Zhong, M; Zhang, C; Luo, J. *Appl. Surf. Sci.*, 2008, 254, 6742-6748.
- [14] Wu, JB; Chen, CY; Shin, CT; Li, MY; Leu, MS; Li, AK. *Thin Solid Films*, 2008, 517, 1141-1145.
- [15] Liu, E; Kwek, HW. *Thin Solid Films*, 2008, 516, 5201-5205.
- [16] Itoh, M; Suda, Y; Bratescu, MA; Sakai, Y. *Thin Solid Films*, 2006, 506-507, 96-100.
- [17] Yap, SS; Tou, TY. *Vacuum*, 2008, 82, 1449-1451.
- [18] Hu, A; Rybachuk, M; Lu, QB; Duley, WW. *Diamond Relat. Mater.*, 2008, 17, 1643-1646.
- [19] Tagawa, M; Yokota, K; Matsumoto, K; Suzuki, M; Teraoka, Y; Kitamura, A; Belin, M; Fontaine, J; Martin, JM. *Surf. Coat. Technol.*, 2007, 202, 1003-1010.
- [20] Trava-Airoldi, VJ; Bonetti, LF; Capote, G; Fernandes, JA; Blando, E; Hubler, R; Radi, PA; Santos, LV; Corat, EJ. *Thin Solid Films*, 2007, 516, 272-276.
- [21] Capote, G; Bonetti, LF; Santos, LV; Trava-Airoldi, VJ; Corat, EJ. *Thin Solid Films*, 2008, 516, 4011-4017.
- [22] Jacob, W. *Thin Solid Films*, 1998, 326, 1-42.
- [23] Shirakura, A; Nakaya, M; Koga, Y; Kodama, H; Hasebe, T; Suzuki, T. *Thin Solid Films*, 2006, 494, 84-91.
- [24] Dearnaley, G. *Clin. Mater.*, 1993, 12, 237-244.

- [25] Thomson, LA; Law, FC; Rushton, N; Franks, J. *Biomaterials*, 1991, 12, 37-40.
- [26] Voevodin, AA; Phelps, AW; Donley, MS; Zabinski, JS. *Diamond Relat. Mater.*, 1996, 5, 1264-1269.
- [27] Zaidi, H; Le, Huu; Paulmier, D. *Diamond Relat. Mater.*, 1994, 3, 787-790.
- [28] Miyoshi, K; Pohlchuck, B; Street, KW; Zabinski, JS; Sanders, JH; Voevodin, AA; Wu, RLC. *Wear*, 1999, 225-229, 65-73.
- [29] Schiffmann, KI; Fryda, M; Goerigk, G; Laure, R; Hinze, P; Bulack, A. *Thin Solid Films* 1999, 347, 60-71.
- [30] Chan, KK; Silva, SRP; Amaratunga, GAJ. *Thin Solid Films*, 1992, 212, 232-239.
- [31] Gehards, I; Ronning, C; Hofsass, H; Seibt, M; Gibhard, H. *J. Appl. Phys.*, 2003, 93 1203-1207.
- [32] Lau, SP; Li, YJ; Tay, BK; Sun, Z; Chen, GY; Ding, XZ. *Diamond Relat. Mater.*, 2001, 10, 1727-1731.
- [33] Hussain, S; Roy, PK; Pal, AK. *Mater. Chem. Phys.*, 2006, 99, 375-381.
- [34] El-Sherbiny, M; Salem, F. *Tribol. Trans.*, 1985, 29, 223-228.
- [35] Roy, R; Sen, SK. *Thin Solid Films*, 1993, 223, 189-195.
- [36] Minton, TK; Garton, DJ. In *Chemical Dynamics in Extreme Environments*, Dressler R; 978-981-02-4177-3; World Scientific, Singapore, SP, 2001, Vol. 11, 1-632.
- [37] Synowki, RA; Hale, JS; Woollam, JA. *J. Spacecraft Rockets*, 1993, 30, 116-119.
- [38] Hedin, AE; Heber, CA; Newton, GP; Spencer, NW; Brinton, HC; Mayr, HG. *J. Geophys. Res-Space*, 1977, 82, 2148-2156.
- [39] Arnold, GS; Peplinski, DR. *AIAA Journal*, 1986, 24, 673-677.
- [40] Park, C. *AIAA Journal*, 1976, 14, 1640-1642.
- [41] Rosner, DE; Allendorf, HD. *AIAA Journal*, 1965, 3, 1522-1523.
- [42] Rosner, DE; Allendorf, HD. *Carbon*, 1965, 3, 153-156.
- [43] Peters, PN; Linton, RC; Miller, ER. *Geophys. Res. Lett.*, 1983, 10, 569-571.
- [44] Tagawa, M; Umeno, M; Ohmae, N. Influence of 5eV atomic oxygen on surface properties of Ag films and graphite. *AIAA paper* 1990, 90-0728.
- [45] Garret, HB; Chutjian, A; Gabriel, S. *J. Spacecraft Rockets*, 1988, 25, 321-340.
- [46] Leger, LJ; Spiker, IK; Kuminecz, JF; Visentine, JT. *AIAA paper*, 1983, 83-2631.
- [47] Leger, LJ; Visentine, JT; Kuminecz, JF. *AIAA paper*, 1984, 84-0548.
- [48] Whitaker, AF. *AIAA paper*, 1983, 83-2632.
- [49] Fraundorf, P; Lindstrom, D; Pailer, N; Sandford, S; Swan, P; Walker, R; Zinner, E. *AIAA paper* 1983, 83-2636.
- [50] Marciano, FR; Bonetti, LF; Pessoa, RS; Marcuzzo, JS; Massi, M; Santos, LV; Trava-Airoldi, VJ. *Diamond Relat. Mater.*, 2008, 17, 1674-1679.
- [51] Zhao, SY; Chen, SH; Li, DG; Ma, HY. *Colloids Surf. A*, 2004, 242, 145-149.
- [52] Sileikaite, A; Prosycevas, I; Puiso, J; Juratis, A; Guobiene, A. *Mat. Sci.*, 2006, 12, 287-291.
- [53] Tuinstra, F; Koenig, JF. *J. Chem. Phys.*, 1970, 53, 1126-1130.
- [54] Dillon, O; Woollam, J; Katkanant, V. *Phys. Rev. B*, 1984, 29, 3482-3529.
- [55] Beeman, D; Silvermann, J; Lynds, R; Anderson, MR. *Phys. Rev. B*, 1984, 30, 870-945.
- [56] Tamorn, MA; Vassell, WC. *J. Appl. Phys.*, 1994, 76, 3823-3828.
- [57] Casiraghi, C; Ferrari, AC; Robertson, J. *Phys. Rev. B*, 2005, 72, 385-401.
- [58] Choi, HW; Dauskardt, RH; Lee, SC; Lee, KR; Oh, KH. *Diamond Relat. Mater.*, 2008, 17, 252-257.

-
- [59] Stoney, GG. *Proc. R. Soc. London, Ser.*, 1909, A 82, 172-175.
- [60] Jacobsohn, LG; Freire Jr, FL. *J. Vac. Sci. Technol., A* 1999, 17, 2841-2850.
- [61] ISO 14577, *Metallic Materials – Instrumented indentation test for hardness and materials parameters*. Part 1: Test method, 2002.
- [62] Oliver, WC; Pharr, GM. *J. Mater. Res.* 1992, 7, 1564-1583.
- [63] Marcuzzo, JS; Urruchi, WI; Massi, M; Grigorov, K; Maciel, HS. *J. Electrochem. Soc.* 2006, 4, 545-552.
- [64] Lieberman, MA; Lichtenberg, AJ. *Principles of Plasma Discharges and Materials Processing*; 0471720011; John Wiley & Sons: New York, NY, 2005; Vol. 1, 1-721.
- [65] Yun, DY; Choi, WS; Park, YS; Hong, B. *Applied Surface Science* 2008, 254, 7925-7928.